Stator Fault Diagnosis of Induction Motor Based on Discrete Wavelet Analysis and Neural Network Technique

Abdelelah Almounajjed[1*], *Ashwin Kumar Sahoo*[1], *Mani Kant Kumar*[2] *and Sanjeet Kumar Subudhi*[1]

(1. Electrical Engineering Department, C.V Raman Global University, Bhubaneswar 752054, India;
2. Electronics and Communication Engineering Department, C.V Raman Global University, Bhubaneswar 752054, India)

Abstract: A novel approach by introducing a statistical parameter to estimate the severity of incipient stator inter-turn short circuit (ITSC) faults in induction motors (IMs) is proposed. Determining the incipient ITSC fault and its severity is challenging for several reasons. The stator currents in the healthy and faulty cases are highly similar during the primary stage of the fault. Moreover, the conventional statistical parameters resulting from the analysis of fault signals do not consistently show a systematic variation with respect to the increase in fault intensity. The objective of this study is the early detection of incipient ITSC faults. Furthermore, it aims to determine the percentage of shorted turns in the faulty phase, which acts as an indicator for severe damage to the stator winding. Modeling of the motor in healthy and defective cases is performed using the Clarke Concordia transform. A discrete wavelet transform is applied to the motor currents using a Daubechies-8 wavelet. The statistical parameters L_1 and L_2 norms are computed for the detailed coefficients. These parameters are obtained under a variety of loads and defects to acquire the most accurate and generalized features related to the fault. Combining L_1 and L_2 norms creates a novel statistical parameter with notable characteristics to achieve the research aim. An artificial neural network-based back propagation algorithm is employed as a classifier to implement the classification process. The classifier output defines the percentage of defective turns with a high level of accuracy. The competency of the adopted methodology is validated via simulations and experiments. The results confirm the merits of the proposed method, with a classification test correctness of 95.29%.

Keywords: Discrete wavelet transform, induction motor, inter-turn short circuit fault, neural networks, statistical parameters

List of symbols

F	Fundamental frequency
p	Number of pole pairs
S	Slip
V_s	Voltage of the stator
R_s	Stator resistance
I_s	Stator current
Ψ_s	Stator flux
R_r	Rotor resistance
I_r	Rotor current
Ψ_r	Rotor flux
L_s	Stator inductance
M_{sr}	Mutual inductance
L_r	Rotor inductance
$i_{\alpha s}$	Stator current on α-axis
$i_{\beta s}$	Stator current on β-axis
$\phi_{\alpha r}$	Rotor flux on α-axis
$\phi_{\beta r}$	Rotor flux on β-axis
$U_{\alpha s}$	Stator voltage on α-axis
$U_{\beta s}$	Stator voltage on β-axis
σ	Leakage coefficient
ω_r	Rotor speed
T_s	Time coefficient on α-axis
T_r	Time coefficient on β-axis
T_e	Electromagnetic torque of IM
f_k	Friction coefficient
J	Moment of inertia
T_{st}	Friction torque of IM
θ_c	Localization parameter
δ	Fault severity index
P_n	Induction motor power

Manuscript received October 19, 2021; revised December 27, 2021; accepted January 19, 2022. Date of publication March 31, 2023; date of current version November 17, 2022.
* Corresponding Author, E-mail: abdelelah_almounajjed@hotmail.com
Digital Object Identifier: 10.23919/CJEE.2023.000003

1 Introduction

Induction motors (IMs) with capacities ranging from a few watts to megawatts are employed as leading movers, and they play an essential role in recent industries. Owing to their robustness, reliability, and low maintenance costs, IMs have received increasing attention in automotive, electrical vehicle traction, and power conversion systems [1-3]. Despite its favorable characteristics, the induction motor is subjected to mechanical and electrical faults that can be caused by prolonged operation, current and voltage imbalance, and harsh operating conditions. If the plant is temporarily shut down for a short period owing to an induction motor fault, it leads to massive economic waste in terms of human resources and raw materials. Therefore, with the increased use of IMs, the search for reliable diagnostic techniques has become a recurrent research task in the recent years. The required techniques aim to diagnose failure at an incipient level to avoid undesirable operating stops [4-6]. In addition, reliable online condition monitoring methods are highly significant for detecting faults during motor operations. These methods are considered necessary to avoid major breakdowns and fault progress, as well as to increase the life span of the motor [7-9].

Stator inter-turn short circuit (ITSC) is a common defect in IMs and accounts for approximately 40% of machine faults. Generally, a few shorted turns do not have remarkable physical indications. However, this may cause immense insulation damage in a short period [10]. Early detection of this fault can minimize the subsequent damage to the adjacent turns and stator core, which would reduce the maintenance cost and motor stop time [11]. Moreover, normal condition monitoring systems are not sufficiently reliable to detect machine faults at a primary evolving level. Therefore, intelligent condition monitoring methods are highly recommended for the initial fault diagnosis and resilient operation of the machine [12].

An ITSC fault creates harmonic frequency components in the motor current. The magnitude and frequency of such harmonics change continuously with the load variations. It is a requisite to identify such faults at suitable frequency bands. Moreover, the selection of a convenient signal processing tool is crucial for effectively analyzing these bands. Fast Fourier transform (FFT), short-time Fourier transform (STFT), and power spectral density (PSD) have been proposed to extract features linked to the fault [13]. During a fault, the motor current signal is nonstationary in nature, which requires an advanced signal-processing tool for analysis. The discrete wavelet transform (DWT) is a preferable tool for dividing stationary and nonstationary signals into different time-frequency resolutions. DWT generates many coefficients for several decomposition levels [14]. The statistical parameters extracted from the DWT coefficients at each decomposition level play a decisive role in the fault diagnosis process. However, recent intelligent fault-diagnosing systems are integral for the detection of motor faults. Recently, special attention has been paid to employing artificial neural networks (ANNs) in the fault diagnosis field. The merits of using an ANN enable arbitrary mapping from inputs to outputs without any concern for the system dynamics, which may be complicated to model in several cases. In addition, the ANN architecture may be performed online with few computational burdens. Note that an ANN can detect faults and estimate their severity without the need to develop a mathematical model. Furthermore, it is highly robust under noisy inputs, and its ability to learn provides a significant advantage in diagnosis and classification processes [15].

The determination of the ITSC fault and its severity has been previously investigated by using several methodologies. In Ref. [16], the authors employed generated approximation signals to estimate the ITSC fault intensity. These signals were obtained after analyzing the raw current signals using the DWT. However, the transient state was ignored during the study, which may have provided crucial information related to the fault. In Ref. [17], a continuous wavelet transform (CWT) was integrated with an ANN to detect ITSC faults. The CWT was utilized to extract relevant features from the measured current signal, and the ANN determined the motor conditions. In the aforementioned work, the input data feeding the ANN were critically small, which affected the accuracy of the results. An online stator ITSC fault diagnosis

method was studied in Ref. [18], using the statistical parameter estimation of the DWT coefficients for detecting faults at an early level. The methodology was performed on a variable-frequency drive that fed the motor in real time. A support vector machine (SVM) was employed as a classifier to detect faults. However, a small number of fault severities were used, and only three loads were used throughout the study. In the study presented in Ref. [4], the failure intensity index was estimated in the faulty phase of a permanent-magnet motor. This method is based on determining the resistance of healthy coils in the defective phase after exciting the machine using a DC current. The resistance value was employed as a feature of the ITSC fault and its severity. The methodology has some errors because of the fact that a short circuit was introduced through wiretaps which have some resistance; however, the algorithm assumed a zero-fault path resistance. The authors of Ref. [19] used the current signal in the time domain to detect the ITSC fault intensity. A neural estimator and multi-agent system (MAS) were employed to determine the fault severity. In Ref. [20], an ANN was chosen as a classifier to estimate ITSC fault severity after processing the amplitude of the motor current signal in the time domain. This study obtained the highest defect classification precision compared to the SVM and fussy logic (FL) techniques. The ITSC fault diagnosis methodology was discussed in Refs. [21-22] based on the discrete wavelet energy ratio. In this study, the classification task was performed using an ANN. In another dimension, the calculation of the energy obtained from DWT does not demonstrate a systematic variance with respect to the augmentation in the failure severity pertaining to the three phases. Furthermore, this random variation in the energy values complicates the ANN pattern, which requires more time to design, train, and test the network to acquire the desired outcomes. In Ref. [23], a pattern recognition method was presented to diagnose ITSC faults by measuring the mutual information among stator current signals. An ANN was used to extract the features and determine the motor condition. A non-invasive method based on infrared thermography was explained in Ref. [24] to detect the presence of an ITSC fault and estimate its intensity. During the start of the motor, the authors employed transient thermal monitoring to perform the diagnostic task. Accordingly, they proposed an algorithm for an automatic ITSC failure diagnosis based on infrared thermography images. The slope of the temperature trend line increases with an increase in fault severity. However, this work was performed under no-load conditions with only two fault conditions. Additionally, this methodology requires at least three minutes to estimate the fault intensity after running the motor. The works presented in Refs. [17-22] cannot estimate fault severity, which only specifies the motor condition as either healthy or faulty. Other studies such as Refs. [20, 24], the fault diagnosis correctness dropped significantly under a few shorted turns in the faulty winding, which adversely affected the overall classification accuracy.

This study is substantially different from the recently published work [25]. A comprehensive comparison of the recent work [25] and the present work includes six aspects. First, to detect the faulty phase, the existing method [25] is based on the max norm values. However, the distinctive features of the L_1 and L_2 parameters were calculated and used in the current study. Second, for fault severity estimation, a mathematical equation approach was used in a previous work [25] without adopting any artificial intelligence technique. An artificial intelligence technique, i.e., ANN, was adopted in this study. Third, the work presented in Ref. [25] focused on calculating the number of faulty turns. In this study, the fault severity was obtained by determining the percentage of shorted turns. Fourth, the proposed method in this work presents an automated method to diagnose faults, compared to the work mentioned in Ref. [25] based on manually calculated mathematical equations. Fifth, to distinguish the defective phase, the L_1 and L_2 parameters employed in this work demonstrate a significant deviation in the value considering the increase in the fault intensity (i.e., L_1: 0-4 000). However, the existing study is based on max norm values, which only range from 185 to 230. Thus, these parameters (L_1 and L_2) provide clearer and more robust indicators of the faulty phase compared to Ref. [25]. Additionally, this clear deviation in the values provides better input to the classifier, which may

increase its performance and accuracy. Finally, to determine the fault severity in the faulty phase, the proposed approach exhibits a higher accuracy compared to that of Ref. [25].

The main contribution of this research is to propose a novel statistical parameter to detect incipient ITSC faults and to specify the percentage of shorted turns in the faulty phase. Furthermore, this study investigated the influence of load variations on fault identification and its intensity. The Clarke Concordia transformation was employed to model the IM for healthy and faulty cases. The DWT-based multi-resolution signal analysis method was used to analyze the motor currents using DB-8 up to the ninth level. The statistical parameters L_1 and L_2 norms were calculated under different loading conditions and fault severities. These norms are combined to constitute the suggested parameter, and their values are selected as relevant features associated with the fault. The aforementioned features are employed to feed the ANN classifier, which precisely determines the motor condition (either healthy or faulty) along with a specific fault intensity.

2 Modeling the induction motor with ITSC fault

Modeling the machine during an ITSC fault is tedious and challenging, particularly without using Park or Clarke transformations. In the healthy case, the stator and rotor equations of the IM are given by Eqs. (1)-(7) [26]

$$U_s = R_s I_s + \frac{\mathrm{d}}{\mathrm{d}t}\psi_s \tag{1}$$

$$0 = R_r I_r + \frac{\mathrm{d}}{\mathrm{d}t}\psi_r \tag{2}$$

$$\psi_s = L_s I_s + M_{sr} I_r \tag{3}$$

$$\psi_r = L_r I_r + M_{sr} I_s \tag{4}$$

To minimize the number of model variables, the motor was represented using the Clarke-Concordia transformation. The general equation of the motor during normal operation is given by

$$\frac{\mathrm{d}}{\mathrm{d}t}x(t) = A(w)x(t) + BU(t) \tag{5}$$

$$x(t) = \begin{bmatrix} i_{\alpha s} \\ i_{\beta s} \\ \phi_{\alpha r} \\ \phi_{\beta r} \end{bmatrix} \quad U(t) = \begin{bmatrix} U_{\alpha s} \\ U_{\beta s} \\ 0 \\ 0 \end{bmatrix} \tag{6}$$

$$\boldsymbol{B} = \begin{pmatrix} \dfrac{1}{L_s\sigma} & 0 \\ 0 & \dfrac{1}{L_s\sigma} \\ 0 & 0 \\ 0 & 0 \end{pmatrix} \tag{7}$$

$$A(w) = \boldsymbol{A}_1 + \omega_r \boldsymbol{A}_2 \tag{8}$$

$$\boldsymbol{A}_1 = \begin{bmatrix} -\left(\dfrac{1}{T_s\sigma}+\dfrac{1-\sigma}{T_r\sigma}\right) & 0 & \dfrac{1-\sigma}{MT_r\sigma} & 0 \\ 0 & -\left(\dfrac{1}{T_s\sigma}+\dfrac{1-\sigma}{T_r\sigma}\right) & 0 & \dfrac{1-\sigma}{MT_r\sigma} \\ \dfrac{M}{T_r} & 0 & -\dfrac{1}{T_r} & 0 \\ 0 & \dfrac{M}{T_r} & 0 & -\dfrac{1}{T_r} \end{bmatrix} \tag{9}$$

$$\boldsymbol{A}_2 = \begin{bmatrix} 0 & 0 & 0 & \dfrac{1-\sigma}{M\sigma} \\ 0 & 0 & -\dfrac{1-\sigma}{M\sigma} & 0 \\ 0 & 0 & 0 & -1 \\ 0 & 0 & 1 & 0 \end{bmatrix} \tag{10}$$

$$\sigma = 1 - \frac{M^2}{L_s L_r} \quad T_s = \frac{L_s}{R_s} \quad T_r = \frac{L_r}{R_r} \tag{11}$$

The torque equation is given by

$$T_e = \frac{PM}{L_r}\left(\phi_{\alpha r} i_{\beta s} - \phi_{\beta r} i_{\alpha s}\right) \tag{12}$$

The expression of the rotor speed is given by

$$\partial\omega r = \frac{P}{J}\left(T_e - T_{st} - \frac{f_k}{P}\omega_r\right) \tag{13}$$

For modeling the IM under an ITSC fault, two parameters were introduced to define this fault. ① Localization parameter θ_c, which represents the angle between the defective phase and reference stator axis (Phase-A). Notably, θ_c can only take the values 0, 2π/3, or 4π/3 according to defective phases A, B, or C, respectively [27]. ② The recognition factor δ, which is the ratio between the number of defective turns and the total number of turns in the healthy phase [26].

The shorted currents of the stator are given by

$$i\alpha\beta sh = \frac{2}{3}\frac{\delta}{R_s}Q(\theta_c)\frac{\mathrm{d}}{\mathrm{d}t}\phi\alpha\beta r \tag{14}$$

The total currents of the stator are given by

$$Y(t) = Cx(t) + D\frac{\mathrm{d}}{\mathrm{d}t}\phi\alpha\beta r \tag{15}$$

Different fault severities can be obtained by changing δ. The tested motor parameters used in this study are listed in Tab. 1. Throughout this work, Phase-C was selected as the faulty phase. For simulating the incipient fault, the number of the defective turns was taken as 1-90 turns, which is less than 20% of the total turns per phase. The simulation was conducted for 6 s. Three-phase currents were recorded in the healthy and faulty cases. These currents were considered under different loading conditions and several fault intensities. Fig. 1 displays the Simulink model of the machine. Fig. 2 illustrates part of the signal of the three-phase motor currents under full load in the time domain.

Tab. 1 Parameters of the utilized machine

Parameter	Value
Number of phases N	3
Source voltage V/V	380
Nominal current I/A	4.4
Motor power P_n/W	2 600
Number of poles P	4
Stator resistance R_s/Ω	4.850
Rotor resistance R_r/Ω	3.805 0
Stator leakage inductance L_s/H	0.274 0
Rotor leakage inductance L_r/H	0.274 0
Mutual inductance M/H	0.258 0
Moment of inertia J/(kg • m^2)	0.031 0
Friction factor f_k	0
Number of turns per stator phase n_s	464
Friction torque T_{st}/(N • m)	0.50

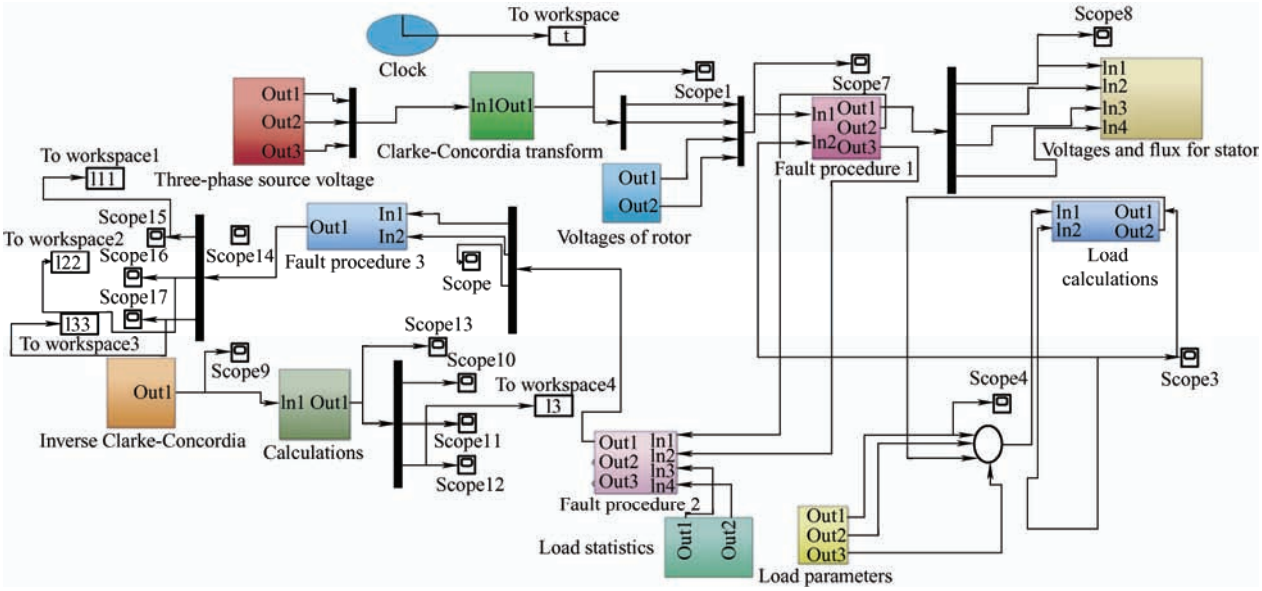

Fig. 1 Simulink model of the machine

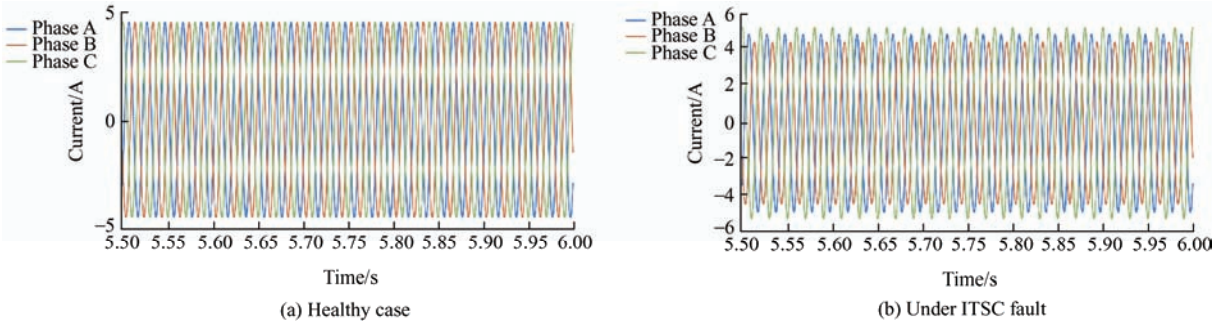

Fig. 2 Three-phase motor currents, under full load (6.3 N • m), in the time domain with ten shorted turns in phase-C

3 Discrete wavelet analysis of stator current

Wavelet transform (WT) is an extension of the short-time Fourier transform (STFT). It analyzes the signals using time-frequency basis functions. A discrete wavelet transform, which utilizes discrete

translation and scaling factors, is obtained when the wavelets are discretely sampled. It samples the shifted and scaled parameters in which the higher-frequency sub-bands have finer time resolution and coarser frequency resolution compared to the lower-frequency sub-bands.

The general equation of wavelet is given by [28]

$$\lambda(t)=\frac{1}{\sqrt{s}}\lambda(\frac{t-u}{s}) \tag{16}$$

where s and u denote the scale and translation factors, respectively.

The DWT uses appropriate filters to divide the current signal into a number of frequency bands to obtain detailed coefficients (D_{cf}) and approximated ones (A_{cf}).

Hence, the approximated and detailed coefficients were obtained by dividing the motor current signal into a number of decomposition levels. The structural decomposition of the DWT for the two levels is depicted in Fig. 3.

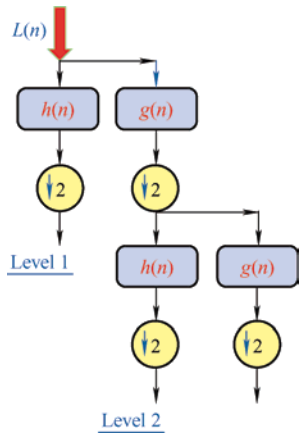

Fig. 3 Structural decomposition of DWT up to the second level

3.1 Discrimination of mother wavelet

The selection of the mother wavelet was the first step in implementing the analysis process. Multiple wavelet families have been proposed with different properties, such as (Haar, Sym2, Sym3, and Db7). Several studies have affirmed that the majority of wavelet families provide acceptable results. However, the Daubechies family is highly recommended for fault diagnosis. The efficacy of using Daubechies wavelets is based on the precise signal reconstruction. Moreover, using a high-order wavelet improves the analysis results, which yields satisfactory outcomes in the diagnosis operation [28-29]. These reasons form the basis for selecting Daubechies-8 as the mother wavelet in this study.

3.2 Determination of the number of decomposition levels

Specifying the number of decomposition levels directly depends on the low-frequency component of the signal. The number of decomposition levels is given by [30]

$$N_f=\text{integer}(\frac{\log\frac{F_s}{f}}{\log 2}) \tag{17}$$

Generally, two additional levels are added for better analysis. The modified equation is as follows

$$N_f=\text{integer}(\frac{\log\frac{Fs}{f}}{\log 2})+2 \tag{18}$$

Generally, the higher the sampling rate, the higher the frequency that a system can record.

In this study, the sampling frequency (F_s) was taken as F_s=10 000 Hz, and the frequency was f=50 Hz.

$$Nf=\text{integer}(\frac{\log\frac{10\,000}{50}}{\log 2})+2=9 \tag{19}$$

Tab. 2 presents the frequency bands of the decomposed signal, for 9 levels.

Tab. 2 Frequency bands of the decomposed signal Hz

Level	Approximations		Details	
1	APPROAX1	0-2 500	D1	2 500-5 000
2	APPROAX2	0-1 250	D2	1 250-2 500
3	APPROAX3	0-625	D3	625-1 250
4	APPROAX 4	0-312.5	D4	312.5-625
5	APPROAX 5	0-156.25	D5	156.25-312.5
6	APPROAX 6	0-78.125	D6	78.12-156.25
7	APPROAX 7	0-39.062	D7	39.06-78.125
8	APPROAX 8	0-19.531	D8	19.53-39.062
9	APPROAX 9	0-9.765 5	D9	9.765-19.531

3.3 Calculating the statistical parameters of wavelet coefficients

Three stator currents were collected from the motor and sampled at a rate of 10 kHz. The DWT was employed to analyze these currents in the healthy and faulty cases (ITSC fault in Phase-C). Db-8 with nine decomposition levels was used for this purpose. Fig. 4 shows the details and approximation signals

(d_9-d_8-d_7-d_6-a_9) for the healthy and faulty Phase-C under full load. It is worth noting from Fig. 4 that the detailed coefficients at level 7 (d_7) have the greatest values compared to the other detailed and approximated coefficients. This is because d_7 contains a fundamental frequency of 50 Hz, as listed in Tab. 2, which demonstrates that d_7 is found at the frequency margin 39-78.1 Hz.

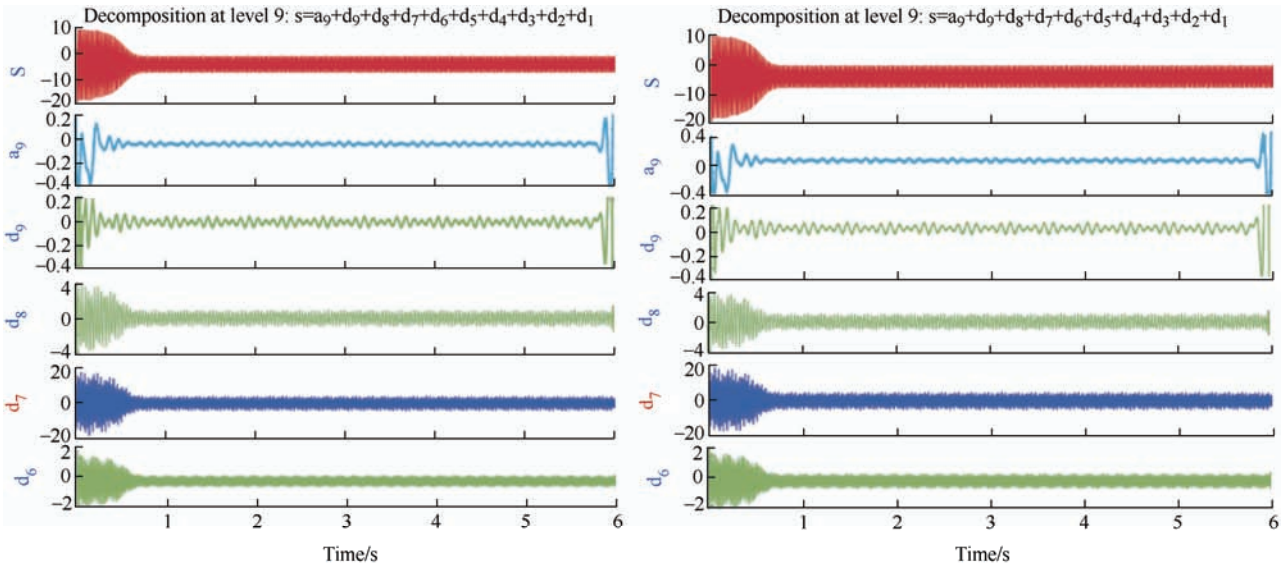

(a) For the healthy case (b) For the faulty case

Fig. 4 Details and approximation signals (d_9-d_8-d_7-d_6-a_9) for Phase-C, under full load (6.3 N • m) with tenshorted turns

These values can result in significant deviations related to the fault. Therefore, these coefficients at the seventh level (d_7) were considered for the fault diagnosis process. To determine the fault features, several statistical parameters are computed for the healthy and faulty cases, such as (L_1 norm, L_2 norm, standard deviation, mean, median, and range). This process was repeated for 17 cases of defective turns. The number of shorted turns ranges from 1-90 turns, which covers the incipient fault (less than 20% of the total turns per phase). Furthermore, at each fault severity, the values of the statistical parameters were recorded under six loading conditions for the three phases. The loading conditions are: 0 N • m, 1.57 N • m, 3.15 N • m, 4.72 N • m, 6.3 N • m, and 7.87 N • m, which correspond to (no-load, 25%, 50%, 75%, 100%, and 125%) of the nominal load, respectively. To select the statistical parameters as a signature of the fault, the variance in the values of the statistical parameters should demonstrate a systematic variation concerning the augmentation of the ITSC fault severity [18]. Subsequently, parameter values were employed to feed the ANN classifier.

4 Proposed ITSC failure detection technique

In this section, three-phase stator currents are acquired, discretized, and processed using the Daubechies-8 wavelet up to the ninth level. The statistical parameters L_1 and L_2 norms were computed for the seventh-level coefficients. These norms are given by

$$L_1 = \sum_{n=1}^{m} | D_7 cf(n) | \tag{20}$$

$$L_2 = \sqrt{\sum_{n=1}^{m} | D_7 cf(n) |^2} \tag{21}$$

where, m represents the total number of coefficients in the seventh level.

In other words, three-phase motor currents were acquired from the IM in a healthy case. The signals obtained were sampled at F_s=10 kHz. These signals were then analyzed using DWT with Db-8, which reached the ninth decomposition level. Subsequently, the statistical parameters L_1 and L_2 norms were only calculated for the seventh decomposition level, as mentioned earlier. This process was iterated for six loading conditions in the healthy case. Hence, for each load condition, three values for L_1 and L_2 were recorded for the three motor phases. Then, for the fault severity 1 shorted turn, the same procedure was repeated, and the results were recorded. Finally, by reaching the final fault severity of 90 shorted turns, the number of collected samples for each L_1 and L_2 norm becomes 324. These samples were arranged for phases

A, B, and C to be ready to feed the classifier.

In the healthy case, the L_1 norm values were equal for all three phases. However, during the fault, the defective Phase-C had the highest values compared to those of the other two healthy ones. The difference in the L_1 value between the defective and healthy phases increases with an increasing ITSC fault severity. This is the same observation as for the L_2 norm. Consequently, L_1 and L_2 norms are considered highly efficient statistical parameters for distinguishing the faulty phase and recognizing fault progress.

To determine the percentage of shorted turns during an incipient fault, the ANN was trained using suitable training data. The training process was performed using L_1 and L_2 norms, in which their values were extracted for the three phases under various loading conditions and several fault severities. Additionally, combining L_1 and L_2 norms creates a new statistic, acquiring the properties of each L_1 and L_2 norms. Moreover, this novel parameter feeds the classifier and the classifier output specifies the machine status.

5 Artificial neural network (ANN) classifier for ITSC fault

An ANN is a computational pattern inspired by the nervous system of living creatures [23]. ANN introduces an informative processing system formed by connecting simple processing units called neurons. These neurons transfer input data using a specific function called the activation function. The connections between the neurons were characterized by weight values. These weights are updated during the training session [17]. The architecture of the multilayer ANN is illustrated in Fig. 5. The principal element of an ANN is the neuron, which can be represented as [20]

$$Z_k(j)=\sum_{m=1}^{n} X_m W_m + b \tag{22}$$

$$Z_k(j)=\phi k(Z_k(j)) \tag{23}$$

where n represents the number of input signals, X indicates the neuron input, W symbolizes the neuron weight, b denotes the bias, $Z_k(j)$ represents the weighted response, and $\phi(\cdot)$ symbolizes the activation function of the neuron.

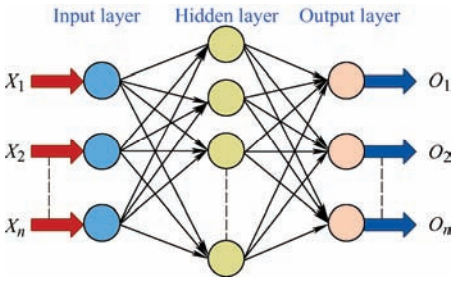

Fig. 5 Architecture of multi-layer ANN

The weights are modified by calculating the error signal. This error is given by

$$E_k(j)=D_k(j)-Y_k(j) \tag{24}$$

where $D_k(j)$ represents the desired output, and $Y_k(j)$ represents the actual output.

Adding the produced errors through the neurons of the ANN may be expressed as

$$Etot(j)=0.5\sum_{m=1}^{P} E_k{}^2(j) \tag{25}$$

where p denotes the number of neurons in the output layer.

An ANN is known for its capability to learn autonomously and generalize nonlinear relationships between output and input variables. This advantage enables the network to find a solution for which other AI techniques fail. In this study, L_1 and L_2 parameters were acquired using the DWT at the seventh decomposition level. These parameters were obtained for the healthy case under six different loading conditions (no-load, 25%, 50%, 75%, 100%, and 125%) of the full load for the three motor phases. Subsequently, this process was repeated for 17 different fault severities, which belong to the range of (1-90) shorted turns. For each fault severity, the values of the aforementioned parameters were recorded for the three motor phases under the previously mentioned loading conditions. These values were then arranged to form the input data to feed the ANN classifier. Hence, for healthy and faulty situations, the network inputs are only L_1 and L_2, which were obtained from the three-phase motor: A, B, and C under six different loads.

The training process was achieved by adjusting the weights of a specific learning rule [21]. The ANN was trained on a well-behaved system. Training continues as long as the network continues to improve the validation. The reference output is compared to the

actual output of the system to isolate the detected anomalies in the system output. The classification process involves the prediction of the class to which an element belongs. Following that, the ANN was tested using a test dataset to validate its performance in the implementation of the required task. A three-layer feed-forward neural network was chosen to diagnose the incipient ITSC fault and its severity. This network was selected as the ITSC fault diagnosis is a complicated nonlinear mapping problem because the inputs and outputs are variables without clear linear relationships. Following the acquisition of the data (L_1 and L_2 values), 70% of the data were trained using ANN for 100 epochs. Therefore, the network parameters were trained. Subsequently, for the detection phase, 30% of the dataset, which is blinded data, is used to evaluate the network performance. This research aims to validate whether the IM is healthy or faulty, along with the estimation of the percentage of defective turns in the faulty phase using an ANN. A flowchart of the machine fault diagnosis process is depicted in Fig. 6.

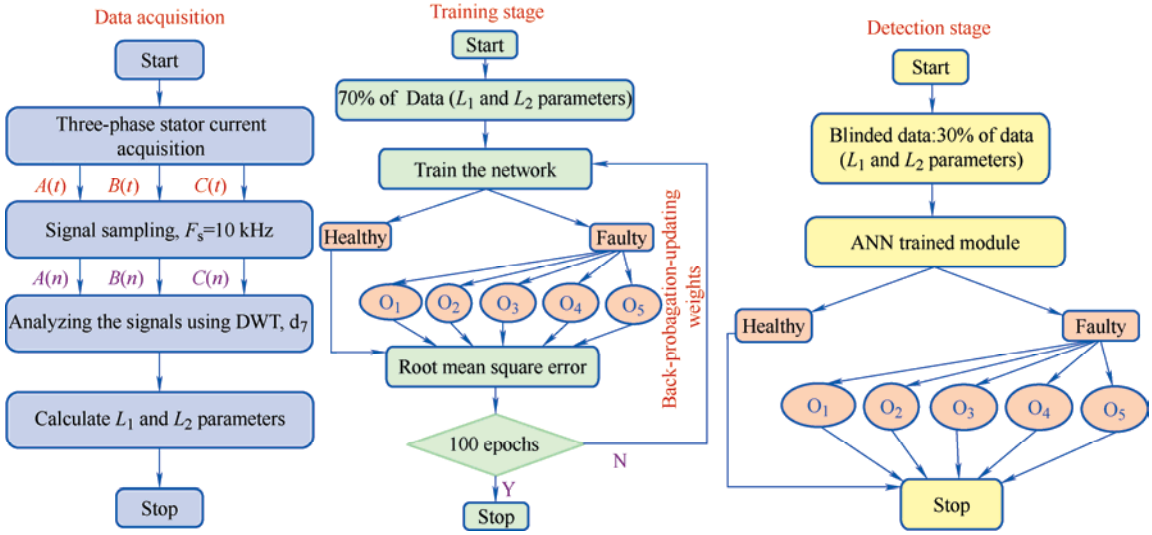

Fig. 6 Suggested stator inter-turn short circuit failure detection algorithm of IM

6 Results and discussion

A squirrel-cage star-connected three-phase IM was chosen to investigate the stator currents for healthy and faulty cases. This study focuses on detecting the stator ITSC fault and determining its severity at an early stage in real time. The robustness of a failure-detection methodology should be measured by diagnosing the fault and estimating its severity under the condition of the least defect intensity. Throughout this research, the failure location is considered in Phase-C.

6.1 Simulation results

The ITSC fault was simulated using the Clarks-Concordia transformation via Matlab/Simulink. To simulate the incipient fault, Phase-C turns are gradually shorted by (1, 3, 5, 7, 10, 13, 15, 17, 20, 23, 25, 35, 45, 55, 65, 80, or 90) turns to obtain various fault intensities. Raw current signals were sampled at a frequency of 10 kHz. DWT was employed to analyze the signals using DB-8 at nine decomposition levels. The detailed coefficients at level 7 were discriminated, and the statistical parameters, L_1 and L_2 norms, were calculated from the coefficients for the three phases. The acquisition time was 6 minutes. The motor worked for 6 s, and then the data were obtained and analyzed for this duration of time.

For the healthy case, the L_1 norm values were equal for the three phases during all loading conditions. The differences in the L_1 norm values between the defective phase and two healthy phases increase when the severity of the ITSC fault is increased. These deviations in values are visible even for the initial fault cases, and the L_1 norm values for Phase-C are greater than those for Phases A and B. Similarly, the same observations were made for the L_2 norm. Consequently, owing to the aforementioned reasons, it is affirmed that L_1 and L_2 norms are suitable to be distinctive features for the diagnosis process. However, other statistics, such as (median, mean, ⋯), are ignored, as

discussed earlier. The validity of applying L_1 and L_2 to the diagnostic process is illustrated in Fig. 7. Distinguishing the defective phase was clear and was directly observed from the L_1 and L_2 values. Indeed, the faulty phase demonstrated the highest values among the other two phases. However, it is not possible to detect the fault intensity from previous values. Therefore, it is necessary to utilize suitable AI technology to implement the classification process.

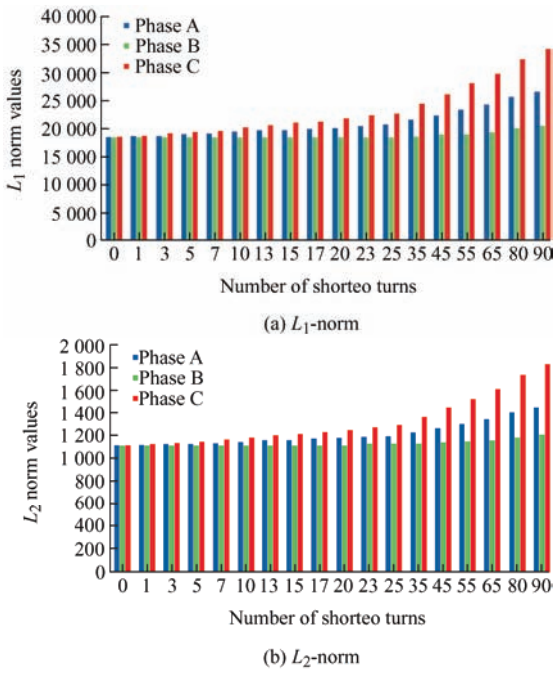

Fig. 7 Variations in the norm values concerning the augmentation in ITSC severity under full load (6.3 N • m), for the three phases

6.1.1 Case 1: Using L_1 norm as an input vector for the classifier

The major difficulties facing the proper use of the ANN include the selection of significant inputs and the choice of network parameters, which make its structure compact to ensure high accuracy. The granted properties presented through the L_1 norm make this parameter highly efficient for feeding and training the classifier. The ANN was performed using Matlab software. This network has a topology with 324 inputs. A single hidden layer consisted of five neurons with a sigmoid transfer function as the activation function. In addition, the network contained six neurons in the output layer with a linear transfer function as the activation function. For the training process, backpropagation was selected as the learning algorithm. All weights were initiated with random values, and the learning rate was 0.1. The configuration parameters used in the ANN are summarized in Tab. 3.

Tab. 3 Configuration parameters utilized in the ANN classifier

Parameter	Value
Number of inputs in case of L_1 or L_2 norm	324
Number of inputs in case of combining L_1 or L_2 norm	648
Activation function of the hidden layer	Sigmoid transfer function
Activation function of the output layer	Linear transfer function
Neurons in the hidden layer	5
Neurons in the output layer	6
Number of epochs	100
Learning rate	0.1
Training algorithm	Back-propagation

(1) Training session. The training data are formed by a successive sequence of samples acquired from the motor under several fault severities and various loading conditions for the three phases. The training data are considered as 70% of the total data, divided into six groups.

Group 1: Twelve samples for the healthy case under six different loads (no-load, 25%, 50%, 75%, 100%, and 125%) of the nominal load.

Group 2: 63 samples representing the ITSC fault of (1, 3, 5, 7 and 10) defective turns in Phase-C, corresponding to fault severity less than 2.5% of the total turns per phase, under six different loads (no-load, 25%, 50%, 75%, 100% and 125%) of the nominal load.

Group 3: 63 samples representing the ITSC fault of (13, 15, 17, 20 and 23) defective turns in Phase-C, corresponding to fault severity less than 5% of the total turns per phase, under six different loads (no-load, 25%, 50%, 75%, 100% and 125%) of the nominal load.

Group 4: 36 samples representing the ITSC fault of (25, 35 and 45) defective turns in Phase-C, corresponding to fault severity less than 10% of the total turns per phase, under six different loads (no-load, 25%, 50%, 75%, 100% and 125%) of the nominal load.

Group 5: 24 samples, representing the ITSC fault of (55 and 65) defective turns in Phase-C, corresponding

to fault severity less than 15% of the total turns per phase, under six different loads (no-load, 25%, 50%, 75%, 100% and 125%) of the nominal load.

Group 6: 24 samples, representing the ITSC fault of (80 and 90) defective turns in Phase-C, corresponding to fault severity less than 20% of the total turns per phase, under six different loads (no-load, 25%, 50%, 75%, 100% and 125%) of the nominal load.

(2) Testing session. In order to evaluate the network performance, the ANN must be tested with a data test set. It is critical to note that during this work, none of the data samples presented for validation or testing were utilized in the training process. The testing and validation data were taken as 102 samples, corresponding to 30% of the total data, as stated earlier. These samples were divided into six groups pertaining to the healthy condition and five different fault severity conditions. They were arranged as follows: 6 samples in Group 1, 27 samples in Groups 2 and 3, 18 samples in Group 4, and 12 samples in Groups 5 and 6. Fig. 8 presents the results of training, validation, testing, and overall accuracy of the classifier using L_1-norm, which reached 91.76%. This percentage represents the classifier's capability to specify the motor condition for the six cases.

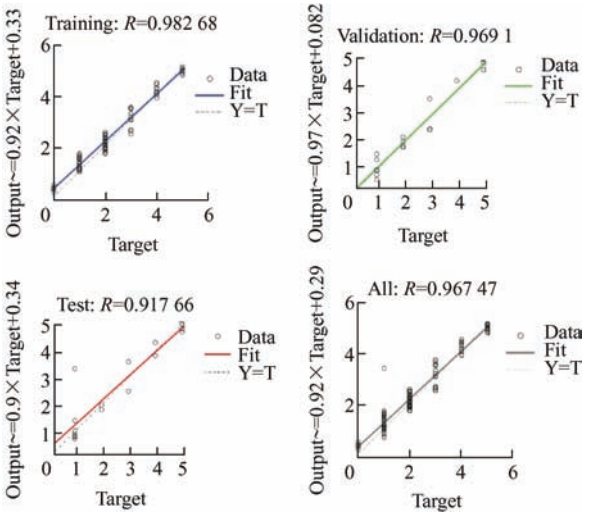

Fig. 8 Results of training, validation, testing, and overall accuracy of the classifier using L_1 norm

6.1.2 Case 2: Using L_2 norm as an input vector for the classifier

The same steps used in Case 1 were iterated here using the L_2 norm values. Fig. 9 illustrates the results of training, validation, testing, and overall accuracy of the classifier using L_2 norm, which reached 93.34%.

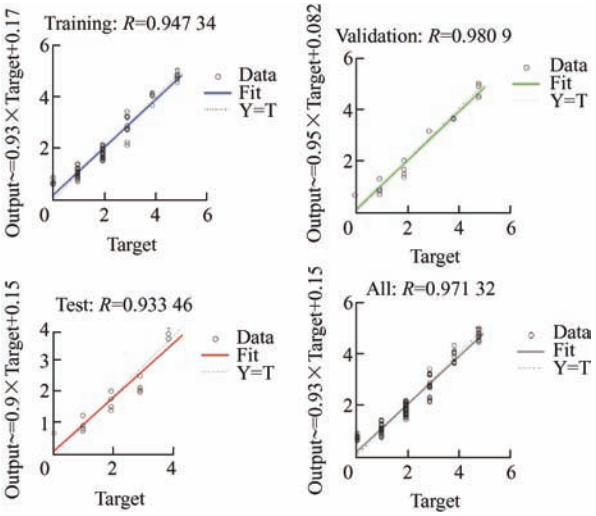

Fig. 9 Results of training, validation, testing, and overall accuracy of the classifier using L_2 norm

6.1.3 Case 3: Using L_1 and L_2 norms together as an input vector for the classifier

Combining L_1 and L_2 norms creates a novel statistic gathering the virtues of using both L_1 and L_2 norms. This process enabled us to obtain the benefit of utilizing double data, which may increase classifier precision. Moreover, employing additional features obtained from the IM provides a better representation of the motor work and makes the fault diagnosis process more generalized compared to previous cases. Consequently, the overall reliability of this procedure is higher than that of applying each norm independently. However, the combination process creates a greater challenge in arranging the input data to feed the classifier.

The same procedures used in Case 1 were repeated; however, the dataset was different. The total data were [(6×6)+(6×17×6)]=648 samples. The training dataset consisted of 456 samples. The validation and testing data comprised 192 samples. Fig. 10 illustrates the results of training, validation, testing, and overall accuracy of the classifier using (L_1+L_2) norm, which reached 95.29%. This percentage represents the classifier's capability to specify the motor conditions for the six cases. The obtained percentage confirms the merit of employing this new norm to feed the classifier with exceptional accuracy.

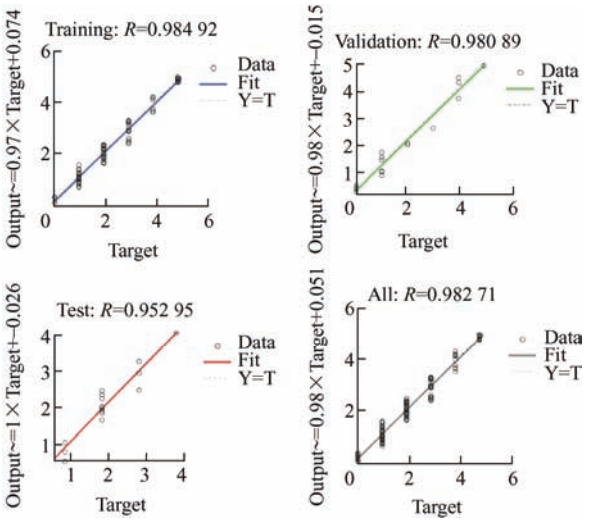

Fig. 10 Results of training, validation, testing, and overall accuracy of the classifier using (L_1+L_2) norm

6.2 Experimental results

In this subsection, an experimental procedure is described to validate the applicability and efficacy of the proposed methodology. The hardware tests were implemented using the hardware setup depicted in Fig. 11 [30]. The figure shows a motor with suitable loading arrangements that were employed to analyze the healthy/defective condition of the IM. The stator of the motor contained six coils with 464 turns per phase. To mimic an ITSC fault, several failures were artificially induced in the winding. Phase-C is considered the faulty phase, which was taken earlier for Simulink. The machine winding was modified and specially wound by adding 17 tappings on the stator coils of Phase C such that the number of defective turns is (1, 3, 5, 7, 10, 13, 15, 17, 20, 23, 25, 35, 45, 55, 65, 80 or 90) turns. The taps are connected to the 1st, 3rd, 5th, 7th, 10th, 13th, 15th, 17th, 20th, 23th, 25th, 35th, 45th, 55th, 65th, 80th or 90th turns. Such a modification process enables an ITSC fault with various numbers of turns in the faulty phase, as depicted in Fig. 12. The motor currents for the three phases were continuously acquired, monitored, and recorded using a LANGLOIS data acquisition system, which was composed of three devices: MECAWATT, WATTELEC, and PCWATT. The MECAWATT device is a display unit that shows three mechanical values of torque, speed, and power, with measurements performed on a rotating induction motor using a torque sensor and a tach generator. Moreover, the WATTELEC equipment includes a digital multimeter with floating inputs that simultaneously display three 3 electric values: voltage, current, and power. Hence, in the hardware experimental procedure, a data acquisition system was used to capture data from the motor at a rate of 10 kHz. Additionally, an RS 232 USB converter was used to connect the PCWATT device to a computer. The purpose of using PCWATT is to record and display mechanical and electrical quantities from a machine on a screen. Subsequently, the data were analyzed using DWT with the same steps utilized in Simulink. In addition, 648 samples were acquired from the three motor phases during the healthy and faulty situations under six loads for both L_1 and L_2 norms. Fig. 13 illustrates the steps adopted for the data acquisition process in the hardware experimental procedure.

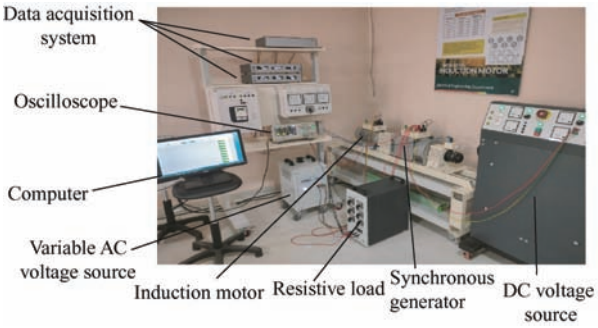

Fig. 11 Experimental setup of the IM with stator ITSC fault

Fig. 12 Rewinding process for the motor winding and testing the tappings, done on the stator coils of Phase-C

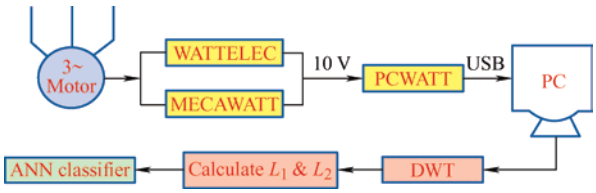

Fig. 13 Steps adopted of the data acquisition process in the hardware procedure

To impair the noise signal, the motor currents were filtered through a low-pass filter with a cutoff frequency of 10 kHz. Similar to the simulation, for each fault severity, six different loading conditions were applied on the motor to enhance the outcome accuracy. The L_1 and L_2 norms were computed from

the experiments and fed to the ANN classifier to validate the motor condition. From the experimental results, the L_1 and L_2 norm values followed the same trend obtained from the simulation. The norm values for the defective phase were greater than those for the other two phases. Moreover, the difference in the values between the faulty and healthy phases also increased as the fault progressed.

During the fault, faulty currents flow unsteadily through the three phases. The defective phase had the highest current. The norm values were acquired after analyzing the faulty currents using the DWT. Hence, the random variations in the motor currents during the fault cause differences in the norm values of the healthy phases A and B.

However, a small deviation in the L_1 and L_2 norm values is noted between the simulation and experiments owing to the noise signals. Fig. 14 presents a comparison of the results obtained from the simulation and experiments.

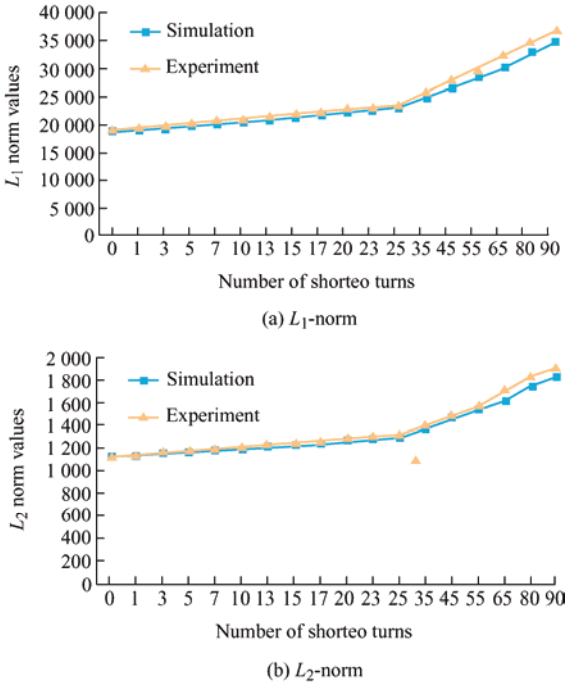

Fig. 14 Comparison between the obtained results from simulation and experiment on Phase-C, under full load (6.3 N • m)

Following the acquisition of the norm values, 648 samples were arranged and fed to the classifier using the same steps used in the simulation. The classifier performance pertaining to its ability to validate the motor status, either healthy or faulty, with a specific fault severity, is listed in Tab. 4. Furthermore, Tab. 4 summarizes the results acquired in this research using a different number of neurons in the hidden layer. As listed in Tab. 4, the classifier test accuracy was increased by adding more neurons to the network.

In this sense, the classification precision was reduced when using five neurons in the hidden layer, compared with ten and seven neurons. However, owing to the relatively limited number of utilized samples, it is important to make the network as simple as possible. A suitable solution is to minimize the number of neurons in the hidden layer to address the purpose of handling problem of overfitting. In other words, the limited number of elements in the training set, in addition to the large number of parameters to be adjusted, can cause an overfitting problem. It adversely affects the reliability of the network and its outcomes. More specifically, without resolving the overfitting problem, the results obtained are meaningless. For this reason, a neural network with five neurons in the hidden layer was selected in this work to implement the classification task. However, the accuracy when utilizing five neurons is still decent and affirms the classifier's ability to perform satisfactorily in the diagnosis process.

From Tab. 4, it is worth noting that the classifier efficiency is uncompromised with respect to the variance in the norm values between the simulation and the experiment. Based on the previous outcomes obtained from the simulation and experiments for the three cases, it can be concluded that the proposed method provides excellent results in the diagnosis and classification process. However, the third case that combines (L_1 and L_2) norms provides the highest test accuracy compared to using each L_1 or L_2 norm separately. The combination process presents a novel statistical parameter with improved efficiency and accuracy in the fault diagnosis process.

Tab. 4 Classifier accuracy for different numbers of neurons in hidden layer

Parameter	10 neurons in hidden layer		7 neurons in hidden layer		5 neurons in hidden layer	
	Simulink accuracy(%)	Experiment accuracy(%)	Simulink accuracy(%)	Experiment accuracy(%)	Simulink accuracy(%)	Experiment accuracy(%)
L_1	97.88	97.47	95.7	95.82	91.76	91.2
L_2	98.52	97.78	95.9	96.21	93.34	93.15
L_1+L_2	99.15	98.81	97.58	96.89	95.29	94.85

7 Comparison with previous papers

Compared to previous works [4, 17-24] pertaining to ITSC fault diagnosis and estimation of its severity, this study presents several significant aspects that should be highlighted.

First, this study is based on statistical parameters that exhibit systematic variation with respect to the increase in fault severity, which significantly affects the performance of the ANN classifier. More specifically, this systematic variation in the norm values simplifies the ANN architecture and increases its efficiency compared to previous works, such as Refs. [21-22].

In addition, in the presented work, the ITSC fault diagnosis and the determination of its intensity are performed online, which enables the capture of any abrupt fault during motor operation. Online condition monitoring refers to the employment of measurement software and hardware to continuously check status of the machine, with the end target of minimizing machine damage, increasing efficiency, and reducing downtime. However, the study presented in Ref. [4] is implemented offline.

Furthermore, it is worth noting that this study demonstrates a high capacity to detect highly incipient faults. These early faults show higher difficulty in differentiating between healthy and faulty cases. However, the studies reported in Refs. [19-20] gave a lower accuracy in detecting such faults.

Furthermore, it is crucial to point out that this methodology demonstrates a type of complexity pertaining to the employment of several steps. These steps include the acquisition of suitable data to determine fault severity, which is considered the most challenging task in this process. Hence, the complexity of the process primarily arises from the acquisition of an appropriate dataset under various situations to arrange the data to feed the classifier, which finally determines the motor status.

Finally, this study was performed under several loading conditions as well as various fault severities. This approach makes the results more generalizable, ascertains the ability of the method to work in several operating situations, and affirms the success of the methodology. However, some studies, such as those in Refs. [17-18, 24] was performed under specific and limited conditions. Tab. 5 summarizes the comparison between the proposed work and previously reported studies.

As summarized in Tab. 5, it is clear that the wavelet transform is currently used as a signal-processing tool to handle the raw signals obtained from the motor. However, the DWT exhibits a greater improvement in this task compared to the continuous version of the wavelet transform (CWT). DWT can derive crucial features linked to the fault, which can then be employed as input vectors to feed various classifiers. In addition, an ANN is utilized to classify the motor condition as either healthy or faulty, as well as to determine the fault severity, as listed in Refs. [17, 20] and this study. Furthermore, a limited number of studies only performed the validation process using both Simulink and the experiment. The Simulink results in this study closely match the experimental results, which affirms the practicality of the proposed methodology. In addition, the matching results give

Tab. 5 Comparison summary of several works reporting stator ITSC failure diagnosis

Literature	Method	Classifier	Load variation	Fault severity estimation	Validation via simulink (S) or experiment (E)	Accuracy of fault severity estimation(%)
Ref. [17]	CWT	ANN	Yes	No	E	—
Ref. [18]	DWT	SVM	Yes	No	S+E	—
Ref. [4]	*D*-axis resistance estimation	—	No	Yes	E	—
Ref. [19]	Current analysis-Time domain	ANN, MAS	Yes	Yes	E	—
Ref. [20]	Current analysis-Time domain	ANN-SVM Fuzzy logic	No	Yes	E	85.79
Ref. [25]	(Wavelet analysis-Max index) +Mathematical equations	—	Yes	Yes	S+E	93.9
Ref. [21]	DWT	ANN	Yes	No	E	—
Ref. [23]	Delayed-mutual information	ANN	Yes	Yes	E	93
Ref. [24]	Infrared thermography	—	No	Yes	E	—
Ref. [22]	DWT	ANN	Yes	No	S	—
Presented work	DWT	ANN	Yes	Yes	S+E	95.09

confidence that the method is almost free of errors pertaining to the simulation or experimental procedure. Moreover, as summarized in Tab. 5, the estimation of the fault severity was performed only for limited works. This particular article demonstrates a higher percentage of the estimation process compared to previously published studies [20, 23, 30].

8 Conclusions

The detection and classification of the initial ITSC fault was performed on an induction motor. The proposed approach can classify the condition of the machine into six categories under different loading conditions and fault severities.

DWT with DB-8 was employed to analyze the raw signals. The combination of the statistical parameters L_1 and L_2 norms of the seventh detailed coefficient is considered as an accurate feature matching to the fault. The fault classification method developed in this study is critically qualified for classifying incipient stator ITSC failure using the ANN classifier.

Finally, the early detection and precise classification of the initial ITSC fault and its intensity using this methodology was completed successfully, with a higher level of accuracy reaching 95.29%.

Besides the scope of this work, the utilized methodology can be generalized to diagnose other faults in the motor, such as a broken rotor bar fault. Moreover, future work can be conducted to diagnose the presence of ITSC in more than one phase.

References

[1] A Almounajjed, A K Sahoo, M K Kumar, et al. Condition monitoring and fault diagnosis of induction motor: An experimental analysis. *In 2021 7th Int. Conf. on Electrical Energy Systems (ICEES)*, 2021: 433-438.

[2] A Almounajjed, A K Sahoo, M K Kumar, et al. Investigation techniques for rolling bearing fault diagnosis using machine learning algorithms. *In 2021 5th Int. Conf. on Intelligent Computing and Control Systems (ICICCS)*, 2021: 1290-1294.

[3] A Almounajjed, A K Sahoo, M K Kumar, et al. Fault diagnosis and investigation techniques for induction motor. *International Journal of Ambient Energy*, 2022, 43(1): 6341-6361.

[4] A Almounajjed, A K Sahoo, M K Kumar. Condition monitoring and fault detection of induction motor based on wavelet denoising with ensemble learning. *Electrical Engineering*, 2022, 104: 2859-2877.

[5] C Y Lee, M S Wen. Establish induction motor fault diagnosis system based on feature selection approaches with MRA. *Processes*, 2020, 8(9): 1-55.

[6] A Almounajjed, A K Sahoo. Wavelet-based multi-class support vector machine for stator fault diagnosis in induction motor. *Transactions of the Institute of Measurement and Control*, 2023, 45(2): 261-273.

[7] F Aghazadeh, A Tahan, M Thomas. Tool condition monitoring using spectral subtraction and convolutional neural networks in milling process. *The International Journal of Advanced Manufacturing Technology*, 2018, 98(9): 3217-3227.

[8] I Zamudio-Ramirez, R A Osornio-Rios, R de J Romero-Troncoso, et al. Wavelet entropy to estimate the winding insulation healthiness in induction motors. *IECON 2019-45th Annual Conference of the IEEE Industrial Electronics Society*, October 14-17, 2019, Lisbon, Portugal. IEEE, 2019, 1: 3716-3722.

[9] H Khelfi, S Hamdani. Induction motor rotor fault diagnosis using three-phase current intersection signal. *Electrical Engineering*, 2020, 102(2): 539-548.

[10] Y Wang, L Yang, J Xiang, et al. A hybrid approach to fault diagnosis of roller bearings under variable speed conditions. *Measurement Science and Technology*, 2017, 28(12): 125104.

[11] G H Bazan, P R Scalassara, W Endo, et al. Stator short-circuit diagnosis in induction motors using mutual information and intelligent systems. *IEEE Transactions on Industrial Electronics*, 2018, 66(4): 3237-3246.

[12] R J Romero-Troncoso, R Saucedo-Gallaga, E Cabal-Yepez, et al. FPGA based online detection of multiple combined faults in induction motors through information entropy and fuzzy inference. *IEEE Transactions on Industrial Electronics*, 2011, 58(11): 5263-5270.

[13] Y Yang, X Dong, Z Peng, et al. Vibration signal analysis using parameterized time-frequency method for features extraction of varying-speed rotary machinery. *Journal of Sound and Vibration*, 2015, 335: 350-366.

[14] J A Antonino-Daviu, M Riera-Guasp, J R Folch, et al. Validation of a new method for the diagnosis of rotor bar failures via wavelet transform in industrial induction machines. *IEEE Transactions on Industry Applications*, 2006, 42(4): 990-996.

[15] Y M Hsueh, V R Ittangihal, W B Wu, et al. Fault diagnosis system for induction motors by CNN using empirical wavelet transform. *Symmetry*, 2019, 11(10): 12-21.

[16] R N Dash, B Subudhi, S Das. Induction motor stator inter-turn fault detection using wavelet transform technique. *IEEE 2010 5th International Conference on Industrial and Information Systems*, 2010: 436-441.

[17] A Jawadekar, S Paraskar, S Jadhav, et al. Artificial neural network-based induction motor fault classifier using continuous wavelet transform. *Systems Science and Control Engineering*, 2014, 2(1): 684-690.

[18] B A Vinayak, K A Anand, G Jagadanand. Wavelet-based real-time stator fault detection of inverter-fed induction motor. *IET Electric Power Applications*, 2020, 14(1): 82-90.

[19] R H C Palácios, I N da Silva, A Goedtel, et al. Diagnosis of stator faults severity in induction motors using two intelligent approaches. *IEEE Transactions on Industrial Informatics*, 2017, 13(4): 1681-1691.

[20] W F Godoy, I N da Silva, A Goedtel, et al. Evaluation of stator winding faults severity in inverter-fed induction motors. *Applied Soft Computing*, 2015, 32: 420-431.

[21] H Cherif, A Benakcha, I Laib, et al. Early detection and localization of stator interturn faults based on discrete wavelet energy ratio and neural networks in induction motor. *Energy*, 2020, 212: 118684.

[22] B Bessam, A Menacer, M Boumehraz, et al. Wavelet transform and neural network techniques for inter-turn short circuit diagnosis and location in induction motor. *International Journal of System Assurance Engineering and Management*, 2017, 8(1): 478-488.

[23] G H Bazan, P R Scalassara, W Endo, et al. Stator fault analysis of three-phase induction motors using information measures and artificial neural networks. *Electric Power Systems Research*, 2017, 143: 347-356.

[24] G Singh, T C A Kumar, V Naikan. Induction motor inter turn fault detection using infrared thermographic analysis. *Infrared Physics and Technology*, 2016, 77: 277-282.

[25] A Almounajjed, A K Sahoo, M K Kumar. Diagnosis of stator fault severity in induction motor based on discrete wavelet analysis. *Measurement*, 2021, 182: 109780.

[26] M Sahraoui, A Ghoggal, S E Zouzou, et al. Modeling and detection of inter-turn short circuits in stator windings of induction motor. *IECON 2006-32nd Annual Conference on IEEE Industrial Electronics*, *IEEE*, 2006: 4981-4986.

[27] S Bachir, S Tnani, J C Trigeassou, et al. Diagnosis by parameter estimation of stator and rotor faults occurring in induction machines. *IEEE Transactions on Industrial Electronics*, 2006, 53(3): 963-973.

[28] S M Hosseini, F Hosseini, M Abedi. Stator fault diagnosis of a BLDC motor based on discretewavelet analysis using ADAMS simulation. *SN Applied Sciences*, 2019, 1(11): 1-13.

[29] B M Ebrahimi, J Faiz, S Lotfi-Fard, et al. Novel indices for broken rotor bars fault diagnosis in induction motors using wavelet transform. *Mechanical Systems and Signal Processing*, 2012, 30: 131-145.

[30] A Bouzida, O Touhami, R Ibtiouen, et al. Fault diagnosis in industrial induction machines through discrete wavelet transform. *IEEE Transactions on Industrial Electronics*, 2010, 58(9): 4385-4395.

Abdelelah Almounajjed received the M.E. degree from Al-Baath University, Homs, Syria, in 2017. He is currently a Ph.D. student in C. V. Raman Global University, Odisha. India. He worked as a lecturer for five years at Al-Baath university. His current research interests are in machine fault diagnosis, signal processing and artificial intelligence applications.

Ashwin Kumar Sahoo, Professor & HOD in the Department of Electrical Engineering, C. V. Raman Global University, Bhubaneswar, Odisha. He has 25 years of teaching & research experience and 2 years of industrial experience. His research interest includes FACTS, microgrid and fault analysis.

Mani Kant Kumar received the M.E. degree from Thapar University, Patiala, India, in 2010 and the Ph.D. degree from Motilal Nehru National Institute of Technology Allahabad (MNNIT Allahabad), Pragayraj, India, in 2019. He is currently working as an assistant professor in the Department of Electronics and Communication Engineering, C. V. Raman Global University, Bhubaneswar 752054, India. His current research interests are in signal processing and nonlinear dynamical systems.

Sanjeet Kumar Subudhi received his B. Tech degree from Silicon Institute of Technology, Biju Pattanaik University of Technology, Odisha, India, in 2008, and M. Tech. degree in Electrical Engineering from Indian Institute of Technology Kharagpur, West Bengal, India, in 2014. Since 2014, he has been working toward the Ph.D. degree in Electrical Engineering Department, National Institute of Technology Rourkela, Odisha, India. Presently, he is working as an assistant professor in Electrical Engineering Department, C. V. Raman Global University, Odisha, India. His research interests include nonlinear dynamics, microgrids, control of switched mode power converters, and power systems.